Hindawi
International Journal of Polymer Science
Volume 2019, Article ID 2603757, 11 pages
https://doi.org/10.1155/2019/2603757

Research Article

Comparison Study between Batch and Continuous Processes to Obtain Chitosan-Based High Porous Biomaterial for Biological Applications

Alina Violeta Ursu, Diana Furtuna, Laura Requia, Safa Larafa, Hélène de Baynast, Philippe Michaud, Gholamreza Djelveh, and Cédric Delattre

Université Clermont Auvergne, CNRS, SIGMA Clermont, Institut Pascal, F-63000 Clermont-Ferrand, France

Correspondence should be addressed to Cédric Delattre; cedric.delattre@uca.fr

Received 23 December 2018; Revised 30 March 2019; Accepted 18 April 2019; Published 15 May 2019

Academic Editor: Domenico Acierno

Foaming process can be monitored under batch or continuous flows conditions. In the batch process, foaming is time-dependent and the foaming efficiency is controlled by the operator. On the other hand, in the continuous process, the foaming efficiency is only monitored by gas and liquid flow rates. The aim of this work is to compare the two technologies to perform porous scaffold biomaterial based on chitosan (a biocompatible polysaccharide) as well as calcium (Ca^{2+}) and silica (SiO_2) (two osteogenesis compounds). Diverse recipes using chitosan (CS) solution (2% (*w*/*v*)) in acetic acid (1% (*v*/*v* in distilled water)) mixed with whey protein isolate (WPI) (2% (*w*/*v*)) as natural surfactant were studied. They were supplemented or not by hydroxyapatite powder (HAp) and tetraethyl orthosilicate (TEOS). A jacketed narrow annular gap unit (NAGU) was used to perform the continuous foaming process. For all experimentations, the mixture flow rate was maintained at 30 mL min^{-1}. The influence of operating conditions such as gas and liquid flow rates was studied to obtain foams and final scaffold material with different densities and porosities. Some other recipes followed foaming under batch conditions. Generally, the recipes were placed in a vessel under mixing allowing the gas phase to come from the roof of the vessel. In this case, it becomes very difficult to control the density and the size distribution of bubbles in the final product. In both cases, liquid foams were analysed (density, bubble size distribution) and then freeze-dried for mechanical and porosity investigations using the dynamic mechanical analysis (DMA) system and scanning electron microscopy (SEM). It has been shown that the controlled injected gas affected the continuous phase, resulting in a lighter and higher porous structure, a more homogeneous appearance, and a more uniform distribution of osteogenesis components compared to one obtained using batch operation. The obtained porous materials exhibited good properties (porosity, interconnectivity, and good HAp and silica distribution) and potential for future bone regeneration applications.

1. Introduction

In the last decades, researchers have given more attention to natural polysaccharides thanks to their interesting properties such as biodegradability, biocompatibility, and stability. Those characteristics allow chitosan (CS) to have great potential to be used in lots of domains such as bone tissue engineering and drug delivery due to its high biocompatibility and fast biodegradation without releasing toxic compounds [1–3]. Nevertheless, biomaterials such as scaffolds made of CS must be porous to be used as biomaterials [3]. Pore size and high interconnectivity between pores have a great influence on foam-based biomaterial properties like mechanical strength and cell adhesion [1–3]. Foam is a dispersion of gas bubbles in a liquid, semiliquid, or solid continuous phase. They are frequently used in the food industry marketed in the form of meringues, whipped cream, or ice cream [4, 5]. Interest in the foam structure can also be found in bio- or mineral materials when looking for acoustic, thermal, or biomedical properties [3, 6]. The presence of gas affects both the mechanical properties and the appearance of the continuous

phase, resulting in a lighter structure, and increased porosity, a more homogeneous appearance, and a more uniform distribution of components within the continuous phase. Successful foaming depends on the combined effect of recipe and process parameters. For example, the viscosity of the recipe should favour gas dispersion but at the same time avoid bubble coalescence. For this reason, the presence of thinking agents such as polysaccharides is required [5, 7, 8]. Moreover, foaming requires surface-active species that must adsorb at the gas–liquid interface to stabilize the system. They can be divided into two classes: (i) low-molecular surfactants (e.g., electrolytes, alcohols, and fatty acids) and (ii) macromolecular surfactants such as proteins which are known to form thick films of considerable mechanical strength that increase the lifetime of foams [7, 8]. Foaming can be done under batch or under steady-state conditions [5, 8, 9]. In the first case, the gas phase comes from the roof of the vessel, so it is usually hard to control the density and size distribution of bubbles in the final product. Continuous manufacturing processes generally use rotor-stator mixing units with small gaps or scraped surface heat exchangers (SSHE) [5, 9]. The main difference between the two devices is that in the first one the mean shear rate is high, but the residence time is short, while in the second the mean shear rate is low, but the residence time is high. These units are high-energy consumers but were commonly used to perform foaming at the industrial scale based only on experimental approach, without any comparison of their performances [5, 8–10]. The operations involving several phases are generally referred to as dispersive mixing. However, foaming operation should be considered as a special case where both dispersive and distributive aspects of gas dispersion should be present. It is clear that both vessel shape and impeller design have to be adapted to take these two aspects into account. An ideal mixer should promote gas dispersion and at the same time mix the fluid efficiently to favour a rapid diffusion [8, 10]. For this purpose, a jacketed narrow annular gap unit (NAGU) was designed as an efficient device to perform foaming under steady-state flow conditions. The device is very simple to design compared to rotor/stator units. However, its performance depends also on the configuration of impellers within the stator.

As example, experimental results showed that a 30° angle shift between two adjacent impellers enhances foaming efficiency (100%) compared to a non-shift or alignment (30%). When aligned configuration was used, the gas phase followed liquid paths within the column; however, the shifted impeller generates a venture effect and enhances gas dispersion through the liquid phase. More details on the effect of impeller design with experimental and numerical approaches are given in Souidi et al. [11, 12]. The present work is aimed at performing the foaming of CS solution alone and with addition of hydroxyapatite (HAp) and/or tetraethyl orthosilicate (TEOS) under steady-state flow conditions using optimum configuration of impellers [11, 12]. The influence of operating conditions—gas/liquid flow rates—on the density and porosity of the final porous biomaterial (scaffold) was investigated. Some experiments have been conducted under batch conditions, however, without monitoring the gas flow rate. The aim was to understand to which extent monitoring the gas flow rate in continuous operation modifies the characteristic of the final product. The aim is not only to obtain foam materials with reliable density, bubble size, and rheological properties but also to afford a simple process permitting to obtain reproducible foam biomaterials with modulated properties (porosity, interconnectivity, density, and mechanical properties) and biological properties due to the presence of osteogenesis agents such as calcium (Ca^{2+} from HAp) and silica (SiO_2 from TEOS) for bone and tissular regenerations.

2. Materials and Methods

2.1. Raw Material Preparation. Foaming experiments were carried out using a raw material that is a mixture of solubilised polysaccharide (foaming agent) and a network former such as a hydroxyapatite mineral filler and/or SiO_2-based glasses from TEOS. The polysaccharide was a low-density CS (France Chitine) with a degree of deacetylation ≥ 90%. First, CS was solubilised in acetic acid 1% (*v*/*v*) at room temperature under stirring for 2 hours and kept overnight at the same temperature. The foaming agent (whey protein isolate or WPI) and the network former (HAp and/or TEOS) were then added under low stirring at room temperature. WPI was added to enhance foaming. WPI (commercially available as Protarmor TM80) was delivered by Armor Proteines (Saint-Brice-en-Coglès, France), and HAp by Sigma-Aldrich (21223) contains calcium phosphate which is known as the best substitute osteogenesis agent for bone regeneration [13]. The mixture was maintained under stirring as HAp is not soluble in CS. Another network formerly used in this study is TEOS employed as SiO_2 precursor. It was largely described in literature for the synthesis of chitosan-silica nanomaterial mediated by the sol-gel mechanism in the acid medium to generate ceramic-like hybrid material for bone regeneration [3, 14]. Then, several recipes using the abovementioned ingredients were prepared using a CS solution of 2% (*w*/*w*) in 1% acetic acid ((*v*/*v*) in distilled water). The CS solution was aged by keeping at room temperature for 24 hours before mixing with other ingredients such as a 2% (*w*/*w*) WPI solution and/or a 5% (*w*/*v*) HAp solution and/or 3% (*w*/*w*) of TEOS (i.e., 1% (*w*/*w*) of the SiO_2 equivalent). Recipes were maintained under low stirring during at least 4 h at room temperature in order to homogenize each ingredient and allow the complete acid hydrolysis of TEOS into SiO_2. The composition and the properties of the formulations used as raw material for foaming processes are presented in Tables 1 and 2.

2.2. Experimental Set-Up for Batch and Continuous Manufacturing of Foams. The recipes (Table 1) were subject to foaming using air as blooming agent by two procedures: (i) in batch process using a rotor-stator device (T 25, ULTRA-TURRAX, Germany) to incorporate air from the roof of the vessel in recipes by mechanically stirring and (ii) in a NAGU (Figure 1) to perform foaming in a continuous

Table 1: Composition of raw material (in % w/v) in acetic acid 1% ((v/v) in distilled water).

Amount of raw material	Notation	Process	
		Batch	Continuous
CS 2%	CS	X	X
CS 2%, WPI 2%	CS/WPI	X	X
CS 2%, WPI 2%, SiO_2 1%	CS/WPI/SiO_2	X	X
CS 2%, WPI 2%, Hap 5%	CS/WPI/HAp	X	X
CS 2%, WPI 2%, SiO_2 1%, HAp 5%	CS/WPI/SiO_2/HAp	ND	X

CS: chitosan; WPI: whey protein isolate; HAp: hydroxyapatite; X: experiment done; ND: no experiment done.

Table 2: Density, rheological properties, and surface tension of raw materials.

Sample	Density ($kg\,m^{-3}$)	Rheological properties			Surface tension ($N\,m^{-1}$)
		n (−)	k (Pa·s^n)	μ (Pa·s)	
CS 2% (w/w)	947	0.94 ± 0.02	0.22 ± 0.02	0.145	52.0 ± 0.6
WPI 2% (w/w)	998	0.99 ± 0.01	0.05 ± 0.001	0.047	44.6 ± 0.1
CS/WPI	958	0.97 ± 0.04	0.50 ± 0.08	0.724	46.0 ± 0.3
CS/WPI/SiO_2	862	0.81 ± 0.01	1.36 ± 0.04	0.464	45.1 ± 0.6
CS/WPI/HAp	954	0.87 ± 0.04	0.89 ± 0.07	0.720	n.d.
CS/WPI/SiO_2/HAp	875	0.71 ± 0.01	3.00 ± 0.15	0.553	n.d.

CS: chitosan; WPI: whey protein isolate; HAp: hydroxyapatite; n.d.: none determined; n: flow behaviour index; k: consistency index; μ: fluid viscosity. Each assay was done in triplicate, and data are expressed as means (± standard deviation).

process controlling gas injection at different flow rates under a given liquid flow rate (30 mL/min).

When the experiment was done in the batch process, the procedure consisted of introducing liquid raw material in a graduated glass cylinder of 200 mL under agitation by a rotor-stator device (T25, ULTRA-TURRAX, Germany) at 10000 rpm until a stable foam is formed (20-25 minutes). The glass cylinder was placed in a cold-water bath, and the temperature was kept close to 4°C.

The volumes of liquid foams were measured, and the foaming ability (FA) parameter was calculated right after the foaming process. As observed in Figure 1, the NAGU was composed of a cylindrical stainless-steel column (35 mm diameter) formed in three jacketed sections 141 mm in height (Figure 1(a)). The configuration permitted to take samples if necessary, from each section of the columns or at the top of the column. Experiments were carried out the day after the preparation of the raw material under steady-state conditions at 4°C. Gas and liquid phases were supplied separately from the bottom of the column using a peristaltic pump (Cole-Parmer Instr. Co., IL, USA) for the raw material and a FC-260 mass flow controller (Tylan, MA, USA) for the gas phase. The liquid flow rate was maintained at 30 mL min^{-1}. Air was used as the gas phase; the low solubility of air in water also improved the stability of small bubbles [4, 7]. The gas flow rate was fixed at 30 mL min^{-1}, 50 mL min^{-1}, or 70 mL min^{-1}, and the rotation speed of the impeller was kept at 600 rpm. The NAGU was mechanically stirred using 21 right-angle paddle mixing elements of 33 mm diameter and 10 mm length (Figure 1(b)). Any gap between two successive elements ($\delta = 0$) shifted at angle $\theta = 30°$ (Figure 1(b)). Such configuration permitted to assure dispersive and distributive aspects of gas dispersion within continuous phases [11, 12]. The jacketed column was thermally regulated (4°C) using cooling fluid connected to a WKL 600 cryothermostat (LAUDA GmbH, Germany).

The exit stream at the top of the column was divided into two parts: one collects foam samples to measure the foam density (ρF), while the other passes through an online image analysis system equipped with an inverted microscope (Axiovert 25, Carl Zeiss Jena GmbH, Germany) and a CDD camera (Kappa Opto-Electronics GmbH, Germany) for the analysis of bubble sizes.

2.3. Measuring Techniques for Raw Material and Liquid Foam Analysis. The raw material was characterized in terms of density, rheological properties, and surface tension. The respective density of the raw material and liquid foams was obtained as the mass-to-volume ratio of each material in a beaker. For foam density measurements, the sampling procedure consisted in collecting carefully the outlet stream in order to fill completely a beaker, the volume and the weight of which were known precisely.

Foam in excess was removed by scraping the surface of the beaker, which limited the structural damage to a small region of foam samples. Three to five samples were necessary to obtain density values with a precision of 2%. The foam

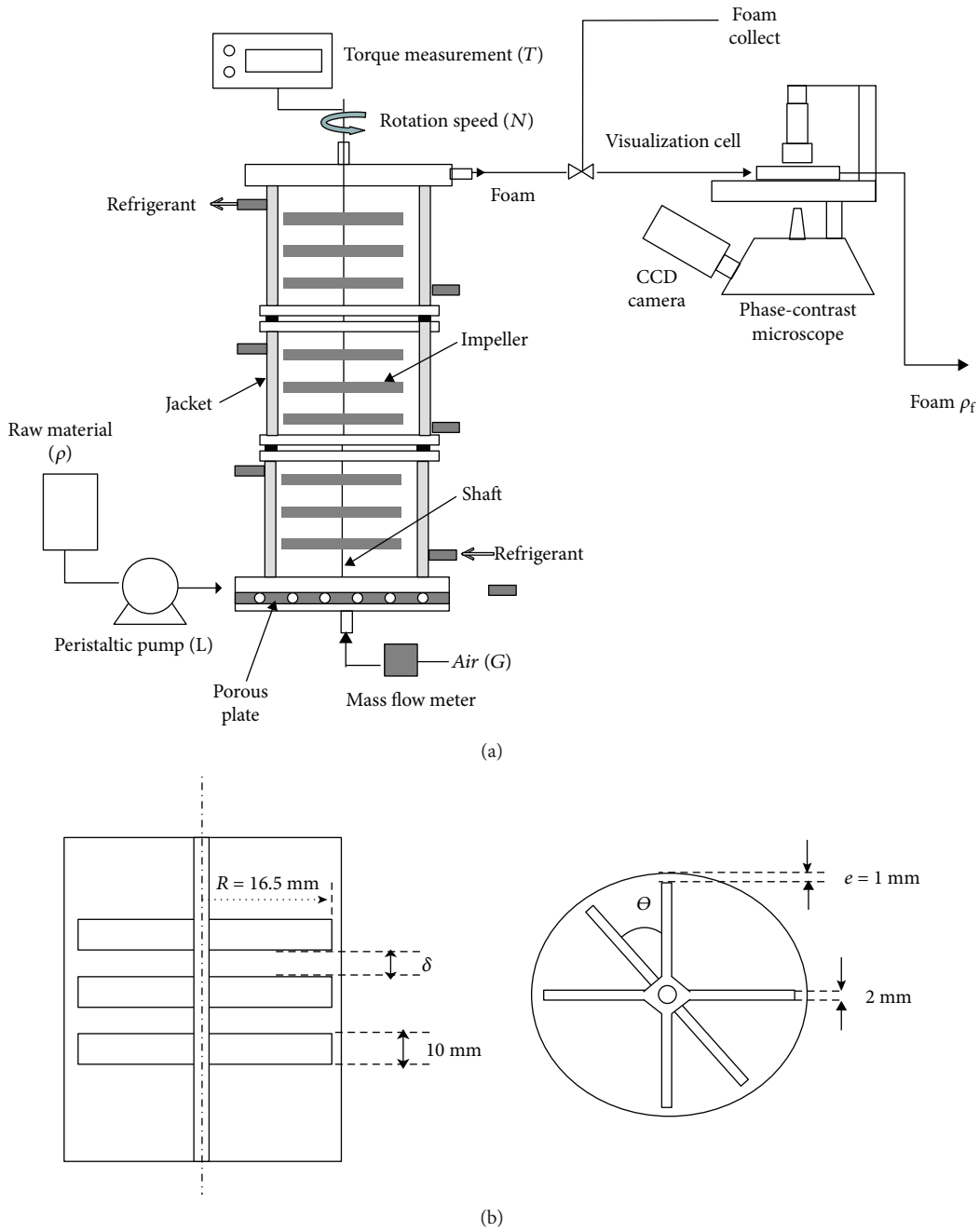

Figure 1: (a) Schematic diagram of a continuous experimental set-up for foam manufacturing and (b) flat-bladed impellers of the NAGU [11, 12].

ability when using batch operation was defined by the following relation (1), in which V_i is the initial liquid volume before foaming and V_f after foaming:

$$\mathrm{FA}(\%) = \frac{V_f - V_i}{V_i}. \quad (1)$$

The efficiency of foaming (Eff) was given only when the operation was done under steady-state flow conditions by

$$\mathrm{Eff} = \frac{\varepsilon_{\mathrm{foam}}}{\varepsilon_{\mathrm{th}}},$$
$$\varepsilon_{\mathrm{foam}} = \frac{\rho L - \rho F}{\rho L}, \quad (2)$$
$$\varepsilon_{\mathrm{th}} = \frac{G}{G+L},$$

where ε_{foam} is the gas volume fraction obtained during foaming and ε_{th} is the theoretical one based on gas (G) and

liquid (L) flow rates (mL min^{-1}); ρL and ρF are, respectively, the liquid and the foam density (kg m^{-3}).

The rheological properties of the materials (initial raw material and liquid foams) were measured using a stress-controlled AR 2000 rheometer (TA Instruments Ltd., UK) equipped with a Peltier circulator for temperature control. Flow rheograms were obtained at the temperature used for foaming experiments (4°C) using a controlled-shear rate, a plate-plate geometry with diameter 50 mm, and a gap of 1 mm. Surface tension of raw material was measured using the Wilhelmy plate method and a K-12 tensiometer (KRÜSS GmbH, Germany). Since the quality of whipped products is closely linked to the characteristics of the dispersed gas phase, such as the mean bubble size and the uniformity of the bubble size distribution [10, 14], image analysis of liquid foams was performed in order to characterize bubble sizes and shapes using a DX-30 camera mounted on an Axiovert 25 microscope with a magnification ratio of 10x. Image Pro-Plus imaging software (Media Cybernetics, MD, USA) was used to count bubbles and estimate bubble size and shape parameters. When the column operated under steady-state conditions, the sampling procedure consisted in collecting online the outlet stream directly in a rectangular quartz cell of 2 mm in width designed to be mounted on the microscope. This procedure prevented bubble loss with time, limited distortion due to structural damage, and provided a constant sample thickness, which resulted in a good sampling reproducibility. As bubbles were spherical, only bubble diameter was measured, and a semi-automated image analysis procedure could be applied [10, 15].

When all the bubbles present in an image were treated, bubble size distribution and average bubble size could be calculated automatically using the Sauter mean diameter d_{32} equation:

$$d_{32} = \frac{\sum_{i=1}^{n} d_i^3}{\sum_{i=1}^{n} d_i^2}, \quad n \in N, \tag{3}$$

which takes both bubble volume and bubble interfacial area into account. Bubble size measurements were generally made on a minimum of five samples that are optical images taken on the fresh foam. To test the repeatability of sampling, the mean bubble diameter was compared, and the difference was generally <5%. At least 100 bubbles were measured in each image, making more than 500 bubbles for each set of operating conditions. This number was shown to be sufficient for statistical analysis by studying the evolution of d_{32} as a function of bubble number.

The stability of liquid foams obtained in batch or in continuous procedure was not an important parameter for this study because the fresh foams were immediately put in a freezer at -80°C to prepare the samples for lyophilization.

2.4. Experimental Set-Up of Scaffold and Morphology Characterization. In batch process conditions, porous scaffolds were made by vacuum freeze-drying of the foams in two steps: the foams were (i) put in a tube (height = 40 mm and diameter = 25 mm) and freeze-dried until -80°C during 24 h and (ii) dried under vacuum at -80°C during 48 h. In continuous process conditions, the foams obtained with various conditions of gas flow rate were lyophilized in the same conditions. The internal morphology of dried porous scaffolds was observed by scanning electron microscopy (JEOL SM820). Before, the samples were cut in the middle by means of a scalpel as shown in Figure 2, and the internal structure was observed far from the edge. They were first attached onto an aluminium stage using a double-sided adhesive. Then, the samples were sputter-coated with a thin gold layer. SEM micrographs were obtained using 15 kV secondary electrons and a working distance of 20 mm. The morphology was observed at 50 and 100x magnification, and the pore sizes of the various prepared scaffolds were analysed at 200x magnification.

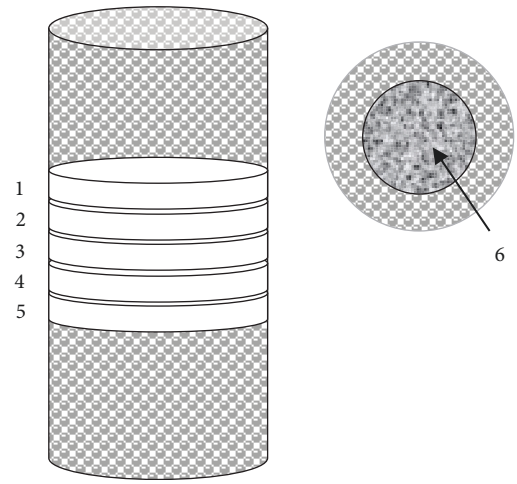

Figure 2: Cutting of the samples. Samples 2 and 4 were for MEB observations, and only part 6 was observed; samples 1, 3, and 5 were for mechanical tests.

The porosity was estimated by the calculation of the gas volume fraction (ε_{SC}) in the scaffold given by

$$\varepsilon_{SC} = \frac{\rho_m - \rho_{SC}}{\rho_m}, \tag{4}$$

where ρ_m and ρ_{SC} are, respectively, the dry mixture and the scaffold density.

The dry mixture density was determined by

$$\rho_m = \frac{\sum_i m_i}{\sum_i m_{i/\rho_i}}, \tag{5}$$

where m_i and ρ_i are the dry mass and the density, respectively, associated to each component i of the scaffold. Densities of raw materials were estimated to be 1340 kg m^{-3} for chitosan, 1050 kg m^{-3} for WPI, 2650 kg m^{-3} for SiO_2, and 3160 kg m^{-3} for HAp.

2.5. Scaffold Mechanical Characterization. To characterize the mechanical properties of chitosan porous scaffolds, the compressive tests were carried out on cutting disks (diameter = 25 mm, thickness = 5 mm) by means of a scalpel as described in Figure 2. Only the central part was observed

to limit the edge effect. The specimens were tested using the DMA 2980 (TA Instruments, France) in compressive mode adding a ramp force of 0.1 to 18 N at a speed of 1 N min^{-1}. The tested specimens were placed between two steel plates to have homogeneous displacement and pressure. The bottom plate was fixed, and the load was applied on the superior surface. The results of the mechanical tests (elongation and compressive stress at break) were analysed through stress-strain curves at 25°C.

3. Results and Discussion

3.1. Raw Material Characterization. Preliminary investigations have shown that CS concentrations equal to 2% (w/v) in acetic acid (1% (v/v) in distilled water) develop a Newtonian behaviour and improve liquid flow through foaming equipment [16]. Consequently, the CS concentration of 2% (w/v) has been used to prepare all the recipes (Table 1). As mentioned in Table 2, addition of WPI does not change the Newtonian behaviour of the CS solution. The mixture of CS/WPI presented a lower surface tension which is well-known as a positive effect for foaming processes.

As observed in Table 2, the addition of SiO_2 and HAp changed the rheological properties of mixtures from a Newtonian behaviour to a pseudo-plastic one. Moreover, the apparent viscosity was determined at a shear rate equal to 1000 s^{-1} (corresponding approximately to 600 rpm in the continuous foaming process using NAGU) using the values of n and k determined by Ostwald's Power Law (Table 2).

Due to the good solubility of the chitosan at pH between 4.0 and 5.0, the formulations used for batch or continuous foaming were maintained at pH 4.5.

3.2. Liquid Foam Characterization

3.2.1. Influence of the Formulation. Liquid foams were characterized using different parameters for products issued by batch and continuous processes. The efficiency of the foaming in the batch procedure was determined by the foaming ability (FA, %) (Table 3) and for the continuous process by evaluation of the density (kg m^{-3}), bubble size (d_{32} (μm)), and foaming efficacy Eff (−) (Table 4).

As well documented in literature, the FA is influenced by several parameters, i.e., the temperature, the impeller configuration and its speed, the nature and the concentration of the foaming agent, the size recipe, etc. [17, 18]. For several decades, the WPI was a reference of the foaming agent notably for the formation/stabilization of food foams. Its foaming properties depend on its ability to absorb at water-air interfaces and prevent coalescence of bubbles. Its functional performances are linked to the protein structure which depends on environmental factors such as pH, ionic strength, and protein concentration [17]. The results (Table 3) showed that the foaming efficiency in the batch process strongly depended on the nature of the formulation. The higher FA (183.3 ± 4.7%) was assigned to a solution of WPI (2% (w/w)) (Table 3). As expected, the CS alone did not develop an interesting FA (FA = 38.2 ± 2.4%) and adding of WPI was mandatory to obtain a better foam formation (FA = 96.7 ± 4.7%). The presence of HAp in the mixtures decreased the FA (e.g., FA = 65.0 ± 2.4% for CS/WPI/Hap vs. FA = 96.7 ± 4.7% for CS/WPI). Visually, the foam structure was very heterogeneous for liquid foams obtained with the batch process (data not shown) with small bubbles on the bottom of the specimen and large bubbles in the surface.

Table 3: Properties of liquid foams obtained in the batch process.

Initial formulation	FA (%)
Solution of CS 2% (w/w)	38.3 ± 2.4
Solution of WPI 2% (w/w)	183.3 ± 4.7
Mixture CS/WPI	96.7 ± 4.7
Mixture CS/WPI/SiO_2	120.0 ± 9.4
Mixture CS/WPI/HAp	65.0 ± 2.4
Mixture CS/WPI/SiO_2/HAp	105.0 ± 11.8

CS: chitosan; WPI: whey protein isolate; HAp: hydroxyapatite; FA: foaming ability. Each assay was done in triplicate, and data are expressed as means (± standard deviation).

Results from Table 4 have shown good foaming efficiency for all formulations from the continuous process using NAGU and revealed the controlled formation of foams with similar rheological properties and closed bubble sizes. One of the most important parameters to evaluate the efficiency of foaming using NAGU is the consistency index k that is related to foam strength. The consistency index increased significantly after foaming ($k > 8.0$ in Table 4 vs. $k \leq 3.0$ in Table 2). Since $n < 1$ (Table 4), all foams produced in the continuous process were classified as pseudoplastic fluids (shear thinning behaviour). For all formulations, the Eff with NAGU (Table 4) was close to 1.00 and the Sauter bubble diameter is similar (d_{32} between 64.25 ± 0.04 μm for CS/WPI/HAp and 70.53 ± 0.01 μm for CS/WPI/SiO_2).

Finally, thanks to online microscopic analysis of foams (Figure 3), the same unimodal bubble distribution was observed for all the mixtures used (i.e., CS/WPI, CS/WPI/-HAp, CS/WPI/SiO_2, and CS/WPI/SiO_2/HAp). The size distributions for all these formulations are close to normal distribution.

3.2.2. Influence of the Gas Flow Rate. To establish the influence of the gas flow rate on the properties of the generated foams, the formulation containing HAp (CS/WPI/HAp) was used. The liquid flow rate (L) and rotating speed (N) were maintained at 30 mL min^{-1} and 600 rpm, respectively. The gas flow rate (G) varied between 30 mL min^{-1} and 70 mL min^{-1}. As observed in Table 5, the increase in the gas flow rate generated (i) a decrease in both the foam flow index n (from 0.66 ± 0.02 to 0.45 ± 0.01) and density (from 528 ± 11 kg m^{-3} to 336 ± 6 kg m^{-3}) and (ii) a very good increase in the consistency index k (from 6.45 ± 0.71 Pa · s^n to 26.42 ± 1.46 Pa · s^n).

The Sauter mean size diameter was higher for the foams obtained by injection of gas with a flow rate equal to 50 mL min^{-1}. Finally, the bubble size distribution was unimodal for all samples (data shown only for CS/WPI/SiO_2) and

Table 4: Rheological properties, density, Eff, and d_{32} of foams obtained using a continuous procedure ($L = 30$ mL min^{-1}, $G = 50$ mL min^{-1}, and $N = 600$ rpm).

Initial formulation	Rheological properties		Density (kg m^{-3})	Eff (−)	d_{32} (μm)
	n (−)	k (Pa·s^n)			
CS/WPI	0.62 ± 0.02	10.0 ± 0.8	382	0.97	66.78 ± 0.01
CS/WPI/SiO_2	0.53 ± 0.01	11.93 ± 0.31	298	1.00	70.53 ± 0.01
CS/WPI/HAp	0.55 ± 0.02	16.12 ± 1.2	402	0.93	64.25 ± 0.04
CS/WPI/SiO_2/HAp	0.61 ± 0.04	8.18 ± 1.42	329	1.00	70.24 ± 0.01

CS: chitosan; WPI: whey protein isolate; HAp: hydroxyapatite; n: flow behaviour index; k: consistency index; Eff: foaming efficacy; d_{32}: bubble size; L: liquid flow rate; G: gas flow rate and N: rotating speed. Each assay was done in triplicate, and data are expressed as means (± standard deviation) or as average value.

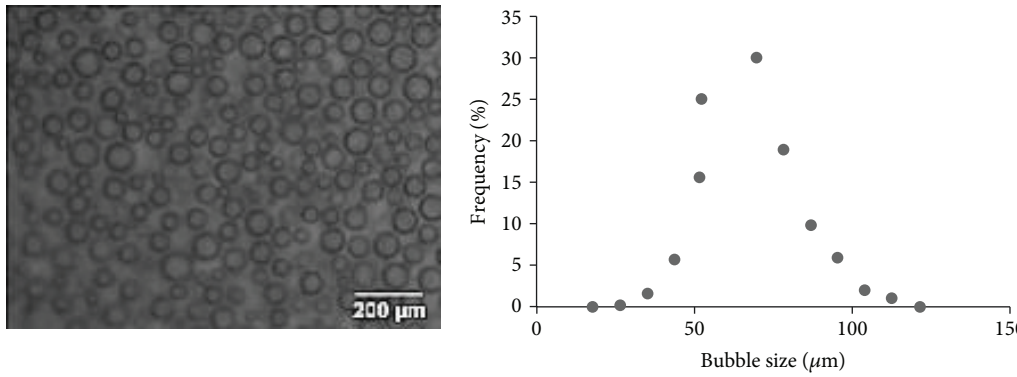

(a) (b)

Figure 3: General bubble distribution analysis of fresh foams obtained using NAGU. (a) Microscopic analysis of fresh foam from the CS/WPI/SiO_2 recipe and (b) bubble size distribution of fresh foam from the CS/WPI/SiO_2 recipe. The same distribution profiles were detected for all recipes (i.e., CS/WPI, CS/WPI/HAp, and CS/WPI/SiO_2/HAp) used (data not shown).

Table 5: Influence of the gas flow rate on the properties of liquid foams obtained in the continuous process using NAGU with the formulation CS/WPI/HAp ($L = 30$ mL min^{-1}, $N = 600$ rpm).

Gas flow rate (mL min^{-1})	Rheological properties		Density (kg m^{-3})	Eff (−)	d_{32} (μm)
	n (−)	k (Pa·s^n)			
30	0.66 ± 0.02	6.45 ± 0.71	528 ± 11	0.89	59.43 ± 0.04
50	0.55 ± 0.02	16.10 ± 1.00	402 ± 15	0.93	64.25 ± 0.04
70	0.45 ± 0.01	26.42 ± 1.46	336 ± 6	0.93	56.05 ± 0.01

CS: chitosan; WPI: whey protein isolate; HAp: hydroxyapatite; n: flow behaviour index; k: consistency index; Eff: foaming efficacy; d_{32}: bubble size; L: liquid flow rate; N: rotating speed. Each assay was done in triplicate, and data are expressed as means (± standard deviation).

statistically close to normal distribution. It should be stated that reducing the mean bubble diameter when increasing the gas flow rate can be explained as follows. The interaction between the gas and liquid phases increases the viscosity and the consistency index of the gas/liquid matrix. According to the capillary number [11, 12], the increases in the viscosity induce the decreases in bubble diameter when mixing takes place in a laminar flow. Note to mention that this was the case observed in the present work.

3.3. Scaffolds and Mechanical Characteristics

3.3.1. Influence of the Formulation. The samples were prepared as described in Experimental Set-Up of Scaffold and Morphology Characterization. The cross-sectional morphology of scaffolds was observed using SEM analysis (Figure 4), and the main properties are summarized in Table 6.

CS scaffolds obtained in batch conditions presented a smooth and porous structure. SEM images show random pores in the range of 100-400 μm with an average diameter of 220 μm and a bad interconnection (Figure 4(a)). It is in accordance with the multilayer sheet structure published in the literature [19, 20]. With the addition of SiO_2, the sheet structure was kept, but SiO_2 agglomerates were formed on the CS matrix (data not shown). Surprisingly, the addition of WPI destroyed the porous structure in the batch process but a spherical shape of pores appeared. The average pore size observed was estimated at 40 μm (Table 6).

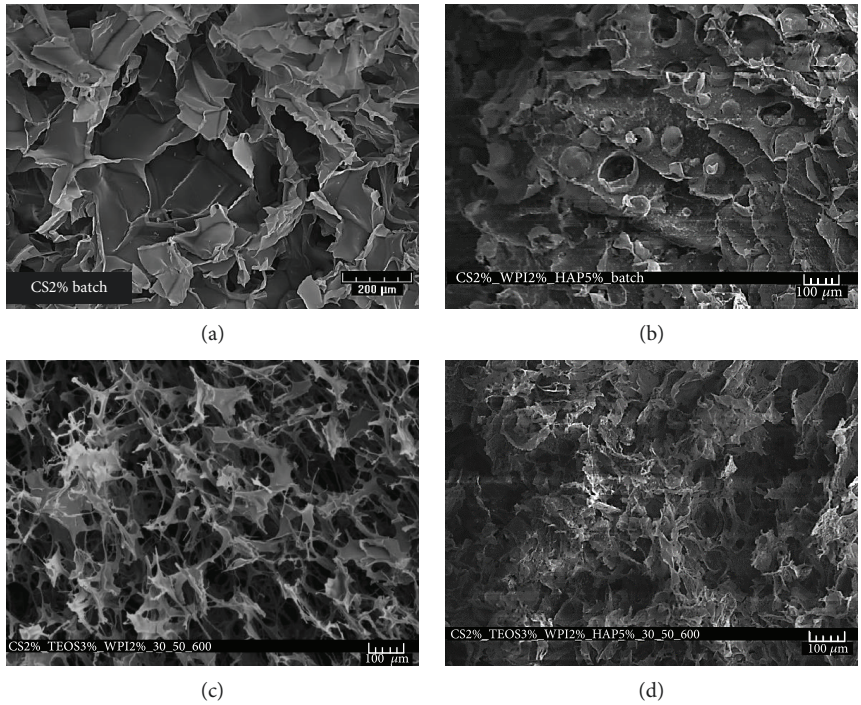

Figure 4: SEM micrographs of the various formulated scaffolds obtained by batch or continuous process ($L = 30$ mL min^{-1}, $G = 50$ mL min^{-1}, and $N = 600$ rpm). (a) CS formulation in the batch process, (b) CS/WPI/HAp formulation in the batch process, (c) CS/WPI/SiO_2 formulation in the continuous process, and (d) CS/WPI/SiO_2/HAp in the continuous process. CS: chitosan; WPI: whey protein isolate; HAp: hydroxyapatite; L: liquid flow rate; G: gas flow rate; N: rotating speed.

Table 6: Pore size and gas volume of fresh foams and scaffolds (dried foam) obtained in batch and continuous procedures ($L = 30$ mL min^{-1}, $G = 50$ mL min^{-1}, and $N = 600$ rpm).

	Batch process		Continuous process (NAGU)			
	Scaffold		Foam		Scaffold	
Formulation	Average pore diameter (μm)	ε_{SC} (%)	d_{32} (μm)	ε_{foam} (%)	Average pore diameter (μm)	ε_{SC} (%)
CS	220	97.26	n.d.	n.d.	n.d.	n.d.
CS/WPI	40 ± 14	95.76	66.78	60.6	110 ± 18	96.6
CS/WPI/SiO_2	n.d.	n.d.	70.53	62.5	n.d.	97.3
CS/WPI/HAp	40 ± 8	97.51	64.25	58.12	98 ± 29	96.85
CS/WPI/SiO_2/HAp	n.d.	n.d.	70.24	62.5	147 ± 34	96.92

CS: chitosan; WPI: whey protein isolate; HAp: hydroxyapatite; ε_{SC}: gas volume fraction in the scaffold; ε_{foam}: gas volume fraction obtained during foaming; d_{32}: bubble size; n.d.: none determined; L: liquid flow rate; G: gas flow rate; N: rotating speed. Each assay was done in triplicate, and data are expressed as the average value.

The loss of pores was even more pronounced with the presence of HAp in the batch procedure, and SEM images showed important agglomerated distribution of HAp (Figure 4(b)). It has already been shown that FA is weaker in the presence of HAp. The porosity obtained from the gas volume fraction (Table 6) was constant whatever the formulation. It lets one think that the sheet structure was kept even in the presence of WPI and HAp and it was the main origin of the porosity of the scaffold. SEM images of CS/WPI/SiO_2/-HAp scaffold (Figure 4(d)) show a nonagglomerated distribution of SiO_2 and HAp into the CS matrix obtained by continuous manufacturing and that the sheet structure was conserved. However, an important increase in spherical pore number was observed. Two sizes of porosities were identified confirming the presence of interconnected structures.

For example, in the case of the CS/WPI/SiO_2/HAp formulation, the diameter of the micropores was in the range of 87–197 μm with an average diameter of 147 μm and an average interconnection diameter of 58 μm. It can be a suitable size for cell nutrient diffusion in and out of the scaffolds [21]. One of the main advantages of the continuous process using NAGU technology is its higher capacity to form controlled spherical and interconnected pores while maintaining the sheet structure of formulated CS. Despite the presence of

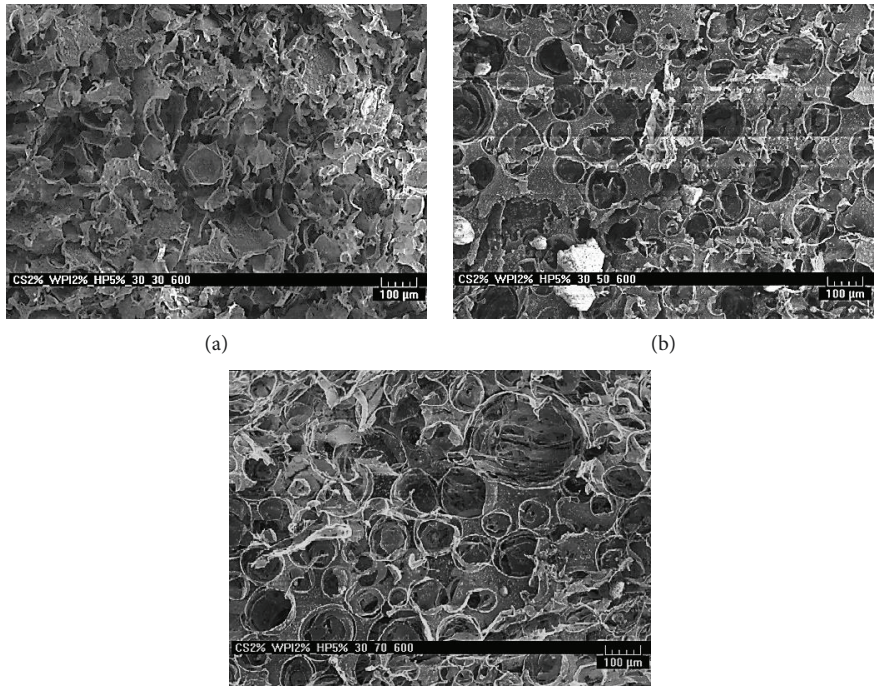

(a) (b) (c)

Figure 5: SEM micrographs of the CS/WPI/HAp scaffold obtained using the continuous process varying gas flow rate incorporation. (a) 30 mL min^{-1}, (b) 50 mL min^{-1}, and (c) 70 mL min^{-1}.

SiO_2 and HAp and the decrease in the foaming ability associated, the gas volumes of scaffolds obtained by the continuous procedure were very constant (controlled injection) and superior to 96% (Table 6). Note to mention that the pore sizes were close to 100 μm.

3.3.2. Influence of the Gas Flow Rate. The impact of the gas flow parameter was observed on the CS/WPI/HAp scaffold morphology (Figure 5) with the objective to generate controlled porous materials. The multilayer sheet structure was maintained with few porosities badly formed for a low gas flow rate (Figure 5(a)).

In this low gas injection condition, pore sizes were polydisperse and the interconnectivity was not clearly observed. However, as illustrated in Figure 5(c), the increase in the gas flow (up to 70 mL min^{-1}) led to the formation of more and more numerous bubble-like pores with a higher controlled monodisperse size (98 μm). A smaller opening was detected between each pore indicating the generation of scaffolds with controlled interconnectivity, more important with a higher gas flow rate (70 mL min^{-1}). The increase in the pore number led to a decrease in the final density of porous scaffold generated under the continuous procedure. In fact, the density was 66.02 ± 3.23 kg m^{-3}, 57.11 ± 0.77 kg m^{-3}, and 42.06 ± 3.23 kg m^{-3} for a gas flow rate of 30 mL min^{-1}, 50 mL min^{-1}, and 70 mL min^{-1}, respectively. In this case, the gas volume fraction varied from 95% to 97.3% which confirmed the controlled production of high porous scaffolds using the continuous procedure (NAGU technology). As a general rule, gas foaming is well known to produce scaffolds with (i) a pore size around 100 μm and porosity up to 92% and (ii) important interconnectivity [22]. Consequently, for the first time we have shown that with NAGU technology, we could create high porous scaffolds with high interconnectivity. Then, this result constitutes a very interesting technological approach for the putative use of these chitosan-based scaffolds for bone regeneration applications.

3.3.3. Scaffold Compressive Strength. A porous material has a viscoelastic behaviour which is an intermediate state between an elastic corpus and an ideal viscous material. The stress-strain curve presents 3 zones [23]. The first zone is a linear zone corresponding to the elastic strain. It is characterized by the flexion of the scaffold walls. The second zone is characteristic of the scaffold walls buckling where the elongation varies strongly with low stress. It is represented by a horizontal plateau. The ultimate zone corresponds to the densification of the scaffold walls. The decrease in the porosity has for consequence the drastic increase in Young's modulus. This was confirmed by the comparison of porosity size and rigidity. For the same formulation of CS/WPI/HAp, the scaffold obtained by the batch process has the smallest porosity size and the biggest rigidity (61.3 kPa) (Figure 6). The scaffold obtained by continuous procedure using NAGU technology presented a lower modulus. The mechanical property optimum corresponds to the conditions $L = 30$ mL min^{-1}, $G = 50$ mL min^{-1}, and $N = 600$ rpm (41.7 kPa). This is to relate to the microstructure of the scaffolds where we observed the better repartition of the bubbles.

As observed, the SiO_2/HAp mixture made drastically rigid the scaffold (Figure 6) which consequently led to a higher elastic modulus value of 73.9 kPa. Scaffold walls were

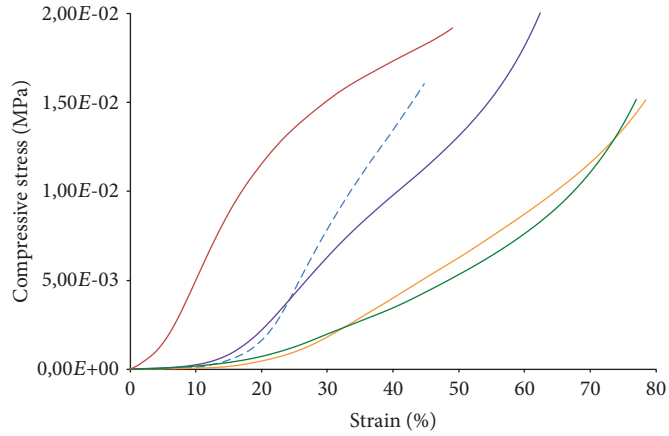

Figure 6: Stress curves in compression mode for the CS/WPI/Hap scaffold obtained by the batch process (dotted blue line) and the CS/WPI/SiO_2/HAp scaffold ($L = 30$ mL min^{-1}, $G = 50$ mL min^{-1}, and $N = 600$ rpm) (full red line), CS/WPI/HAp scaffold ($L = 30$ mL min^{-1}, $G = 50$ mL min^{-1}, and $N = 600$ rpm) (full violet line), CS/WPI/HAp scaffold ($L = 30$ mL min^{-1}, $G = 30$ mL min^{-1}, and $N = 600$ rpm) (full orange line), and CS/WPI/HAp scaffold ($L = 30$ mL min^{-1}, $G = 70$ mL min^{-1}, and $N = 600$ rpm) (full green line) obtained by foaming continuous process using NAGU technology.

very thin, and the characteristic zone of buckling was not observable. However, curves marked an inflexion corresponding to the densification zone around a strain of 30-50%. Beyond, scaffolds presented an important densification. Except for CS/WPI/SiO_2/HAp formulation, the first zone described above is not observable. The low value of Young's modulus means that the scaffold had a very elastic behaviour and was soft and flexible. Consequently, all these mechanical behaviours constitute very interesting properties for future applications in bone tissue engineering [13, 24].

4. Conclusion

Chitosan is a biosourced and biodegradable polymer with great potential as a nontoxic and biocompatible material. However, it has been poorly investigated at this time in the field of highly porous biomaterial for bone regeneration. In this study, two processes were developed to manufacture porous chitosan/hydroxyapatite/tetraethyl-orthosilicate-based materials with the objective to make porous scaffolds including in their structures osteogenesis agents (Ca^{2+} and SiO_2). Several formulations including (or not) emulsifying agents were treated using the batch or continuous foaming process. The foaming ability of liquid foams was strongly influenced by formulations, the higher foaming abilities being obtained with WPI and the lower with CS. With the CS/WPI/HAp formulation used as a model, the increase in the gas flow rate in the continuous process (NAGU technology) led to a higher average pore diameter compared to that obtained with the batch one. Note also the decrease in this bubble diameter when the gas flow rate increased due to an increase in viscosity. The most homogeneous porous scaffolds with the best porosity, pore distribution, interconnectivity, and distribution of osteogenesis agents (Ca^{2+} and SiO_2) were also obtained with the continuous foaming process applied to the CS/WPI/SiO_2/HAp formulation. Interestingly, a very good homogeneous distribution of Ca^{2+} and SiO_2 on the surface and inside the pores was observed in this high porous CS-based foam material. The obtained biomaterials from this formulation had the higher value of Young's modulus compared to those not including SiO_2 which had an elastic behaviour. This innovative continuous foaming process opens the way to the generation of porous biomaterials more or less flexible with controlled porosity as a ceramic-like foam mimetic of the bone structure. Work is in progress to explore and confirm the biological and mechanical performances of these porous materials for bone regeneration applications.

Data Availability

The data used to support the findings of this study are available from the corresponding author upon request.

Conflicts of Interest

The authors declare that there are no conflicts of interest to declare.

References

[1] C. Delattre, "Opinion about advances of chitosan in pharmaceutical field: from past to now," *Modern Applications in Pharmacy & Pharmacology*, vol. 1, no. 1, pp. 1–3, 2017.

[2] N. Mati-Baouche, P. H. Elchinger, H. de Baynast, G. Pierre, C. Delattre, and P. Michaud, "Chitosan as an adhesive," *European Polymer Journal*, vol. 60, pp. 198–212, 2014.

[3] C. Laroche, C. Delattre, N. Mati-Baouche et al., "Bioactivity of chitosan and its derivatives," *Current Organic Chemistry*, vol. 22, no. 7, pp. 641–667, 2018.

[4] G. M. Campbell, C. Webb, S. S. Pandiella, and K. Niranjan, *Bubbles in Food*, Eagan Press, St. Paul, MN, USA, 1999.

[5] R. K. Thakur, C. Vial, and G. Djelveh, "Effect of composition and process parameters on elasticity and solidity of foamed

food," *Chemical Engineering and Processing: Process Intensification*, vol. 47, no. 3, pp. 474–483, 2008.

[6] D. P. Biswas, P. A. Tran, C. Tallon, and A. J. O'Connor, "Combining mechanical foaming and thermally induced phase separation to generate chitosan scaffolds for soft tissue engineering," *Journal of Biomaterials Science, Polymer Edition*, vol. 28, no. 2, pp. 207–226, 2017.

[7] E. Dickinson and G. Stainsby, *Colloid in Food*, Applied Science, London, 1982.

[8] R. K. Thakur, C. Vial, and G. Djelveh, "Foaming of commercial grade food products in a continuous stirred column," *Chemical Engineering Research and Design*, vol. 81, no. 9, pp. 1083–1089, 2003.

[9] R. K. Thakur, C. Vial, K. D. P. Nigam, E. B. Nauman, and G. Djelveh, "Static mixers in the process industries-a review," *Chemical Engineering Research and Design*, vol. 81, no. 7, pp. 787–826, 2003.

[10] M. Labbafi, R. K. Thakur, C. Vial, and G. Djelveh, "Development of an on-line optical method for assessment of the bubble size and morphology in aerated food products," *Food Chemistry*, vol. 102, no. 2, pp. 454–465, 2007.

[11] K. Souidi, A. Mardaru, M. Roudet, A. Marcati, D. Della Valle, and G. Djelveh, "Effect of impellers configuration on the gas dispersion in high-viscosity fluid using narrow annular gap unit. Part 1: experimental approach," *Chemical Engineering Science*, vol. 74, pp. 287–295, 2012.

[12] A. Mardaru, K. Souidi, A. Marcati et al., "Effect of impellers configuration on the gas dispersion of high-viscosity fluid using narrow annular gap unit. Part 2: numerical approach," *Chemical Engineering Science*, vol. 75, pp. 63–74, 2012.

[13] J. I. González Ocampo, D. M. Escobar Sierra, and C. P. Ossa Orozco, "Porous bodies of hydroxyapatite produced by a combination of the gel-casting and polymer sponge methods," *Journal of Advanced Research*, vol. 7, no. 2, pp. 297–304, 2016.

[14] T. M. Budnyak, I. V. Pylypchuk, V. A. Tertykh, E. S. Yanovska, and D. Kolodynska, "Synthesis and adsorption properties of chitosan-silica nanocomposite prepared by sol-gel method," *Nanoscale Research Letters*, vol. 10, no. 1, pp. 1–10, 2015.

[15] C. Vial, R. K. Thakur, G. Djelveh, and L. Picgirard, "Continuous manufacturing of a light-textured foamed fresh cheese by dispersion of a gas phase. I. Influence of process parameters," *Journal of Food Engineering*, vol. 77, no. 1, pp. 1–13, 2006.

[16] N. Mati-Baouche, H. de Baynast, C. Vial et al., "Physico-chemical, thermal, and mechanical approaches for the characterization of solubilized and solid state chitosans," *Journal of Applied Polymer Science*, vol. 132, no. 2, article 41257, 2015.

[17] J. D. Firebaugh and C. R. Daubert, "Emulsifying and foaming properties of a derivatized whey protein ingredient," *International Journal of Food Properties*, vol. 8, no. 2, pp. 243–253, 2005.

[18] B. Zhu, Q. Song, J. Liu, J. Liu, W. Gao, and L. Li, "Effects of foaming parameters on sized-foam properties," *Textile Research Journal*, vol. 86, no. 19, pp. 2096–2105, 2016.

[19] B. H. Atak, B. Buyuk, M. Huysal et al., "Preparation and characterization of amine functional nano-hydroxyapatite/chitosan bionanocomposite for bone tissue engineering applications," *Carbohydrate Polymers*, vol. 164, pp. 200–213, 2017.

[20] G. Li, Q. Xiao, L. Zhang, Y. Zhao, and Y. Yang, "Nerve growth factor loaded heparin/chitosan scaffolds for accelerating peripheral nerve regeneration," *Carbohydrate Polymers*, vol. 171, pp. 39–49, 2017.

[21] L. Baldino, S. Cardea, I. De Marco, and E. Reverchon, "Chitosan scaffolds formation by a supercritical freeze extraction process," *The Journal of Supercritical Fluids*, vol. 90, pp. 27–34, 2014.

[22] S. Preethi Soundarya, A. Haritha Menon, S. Viji Chandran, and N. Selvamurugan, "Bone tissue engineering: scaffold preparation using chitosan and other biomaterials with different design and fabrication techniques," *International Journal of Biological Macromolecules*, vol. 119, pp. 1228–1239, 2018.

[23] M. F. Ashby and R. F. M. Medalist, "The mechanical properties of cellular solids," *Metallurgical Transactions A*, vol. 14, no. 9, pp. 1755–1769, 1983.

[24] Q. Lv and Q. Feng, "Preparation of 3-D regenerated fibroin scaffolds with freeze drying method and freeze drying/foaming technique," *Journal of Materials Science: Materials in Medicine*, vol. 17, no. 12, pp. 1349–1356, 2006.